Photoacoustic determination of the speed of sound in single crystal cyclotrimethylene trinitramine at acoustic frequencies from 0.5 to 15 GHz

Citation: Johnson, Jeremy A., Kara J. Manke, David G. Veyssett, A. A. Maznev, Kyle J. Ramos, Daniel E. Hooks, and Keith A. Nelson. "Photoacoustic determination of the speed of sound in single crystal cyclotrimethylene trinitramine at acoustic frequencies from 0.5 to 15 GHz." Journal of Applied Physics 110, no. 11 (2011): 113513. © 2011 American Institute of Physics.

As Published: http://dx.doi.org/10.1063/1.3667291

Publisher: American Institute of Physics

Persistent URL: http://hdl.handle.net/1721.1/82529

Version: Final published version: final published article, as it appeared in a journal, conference proceedings, or other formally published context

Photoacoustic determination of the speed of sound in single crystal cyclotrimethylene trinitramine at acoustic frequencies from 0.5 to 15 GHz

Jeremy A. Johnson, Kara J. Manke, David G. Veysset, A. A. Maznev, Kyle J. Ramos, Daniel E. Hooks, and Keith A. Nelson

Citation: Journal of Applied Physics **110**, 113513 (2011); doi: 10.1063/1.3667291
View online: http://dx.doi.org/10.1063/1.3667291
View Table of Contents: http://scitation.aip.org/content/aip/journal/jap/110/11?ver=pdfcov
Published by the AIP Publishing

Photoacoustic determination of the speed of sound in single crystal cyclotrimethylene trinitramine at acoustic frequencies from 0.5 to 15 GHz

Jeremy A. Johnson,[1,a)] Kara J. Manke,[1] David G. Veysset,[1] A. A. Maznev,[1] Kyle J. Ramos,[2] Daniel E. Hooks,[2] and Keith A. Nelson[1]
[1]*Department of Chemistry, Massachusetts Institute of Technology, Cambridge, Massachusetts 02139, USA*
[2]*Los Alamos National Laboratory, Los Alamos, New Mexico 87545, USA*

(Received 7 July 2011; accepted 5 November 2011; published online 7 December 2011; corrected 9 February 2012)

We report photoacoustic measurements of the quasi-longitudinal speed of sound along different crystallographic directions in the energetic molecular crystal cyclotrimethylene trinitramine (RDX). Measurements in (100)-oriented RDX were made using two complimentary techniques to probe acoustic frequencies from 0.5 to 15 GHz to resolve large discrepancies in reported sound speed values measured using different techniques and frequency ranges. In impulsive stimulated light scattering (ISS), two laser beams were crossed at various angles in a sample to generate coherent acoustic waves with well-defined wavevectors. Picosecond acoustic interferometry (PAI) measurements were conducted in which a laser pulse heated a thin metal transducer layer coated on the sample surface to generate a broadband acoustic wave-packet that propagated into the sample. Time-dependent coherent Brillouin scattering of probe light from the acoustic waves revealed frequencies in the 0.5–3.5 GHz range in ISS measurements and at ~15 GHz in the PAI measurements, yielding the speed of sound in each case. Our ISS results are in agreement with previous ultrasonic and ISS measurements at kilo- and megahertz frequencies. Our PAI results yielded a 15 GHz sound speed essentially equal to those at megahertz frequencies in contrast to an earlier report based on Brillouin light scattering measurements. The lack of acoustic dispersion over six orders of magnitude in frequency indicates that there is no relaxation process that significantly couples to acoustic waves in RDX at acoustic frequencies up to 15 GHz. © *2011 American Institute of Physics*. [doi:10.1063/1.3667291]

I. INTRODUCTION

The mechanisms through which energetic materials undergo initiation of detonation have been the subject of much experimental and theoretical effort.[1–3] Mechanical shock induces detonation in many energetic materials, posing challenging questions as to how high-energy, microscopic bond breaking can be triggered by low-energy, long-wavelength acoustic modes, associated more with macroscopic material properties rather than microscopic chemical dynamics. Coupling between acoustic modes and other lattice and molecular degrees of freedom clearly plays a crucial role. This can be revealed in part through frequency-dependent dispersion in the elastic properties that arises close to acoustic frequencies that coincide with energy relaxation rates of coupled higher-frequency modes. Many energetic materials are molecular crystals with low crystal symmetry and anisotropic mechanical properties. Determination of their frequency-dependent elastic constants is important for modeling of their dynamical responses and may indicate the extent of interactions between acoustic modes and other degrees of freedom.

A number of methods have been employed to measure the elastic constants in anisotropic crystals in different acoustic frequency ranges from kilo- to gigahertz.[4–8] Often there is no practical difference between the resulting elastic constants regardless of the experimental frequency range or measurement technique, but recent studies of energetic materials by Brillouin light scattering (BLS) at ~10–20 GHz acoustic frequencies[9,10] have yielded intriguing discrepancies with ultrasonic measurements performed at kilohertz frequencies.[11,12] In particular, the longitudinal elastic modulus C_{11} of cyclotrimethylene triamine (RDX) measured by BLS[9] was reported to be 40% higher, whereas C_{42} was six times lower compared to the ultrasonic data.[11,12]

The reported discrepancies point to a possible relaxation mechanism that would result in dispersion and thus frequency-dependent elastic constants. When relaxation that couples to acoustic modes, for example vibrational relaxation in molecular gases[13] and liquids,[14] is on a time scale τ much faster than the acoustic period, the acoustic wave will propagate as if there is no coupling of modes. But when the relaxation time becomes coincident with or slower than the acoustic period, coupling will result in acoustic dispersion. The speed of sound at high frequencies ($\omega\tau \gg 1$) will be different than the speed of sound at low frequencies ($\omega\tau \ll 1$). For the simplest case of a single exponential (Debye) relaxation, the dispersive region will span more than one decade in frequency.

The discrepancies in reported RDX elastic constants led Sun *et al.*[15] to address the issue of potential relaxation

a)Author to whom correspondence should be addressed. Electronic mail: jeremyj@mit.edu.

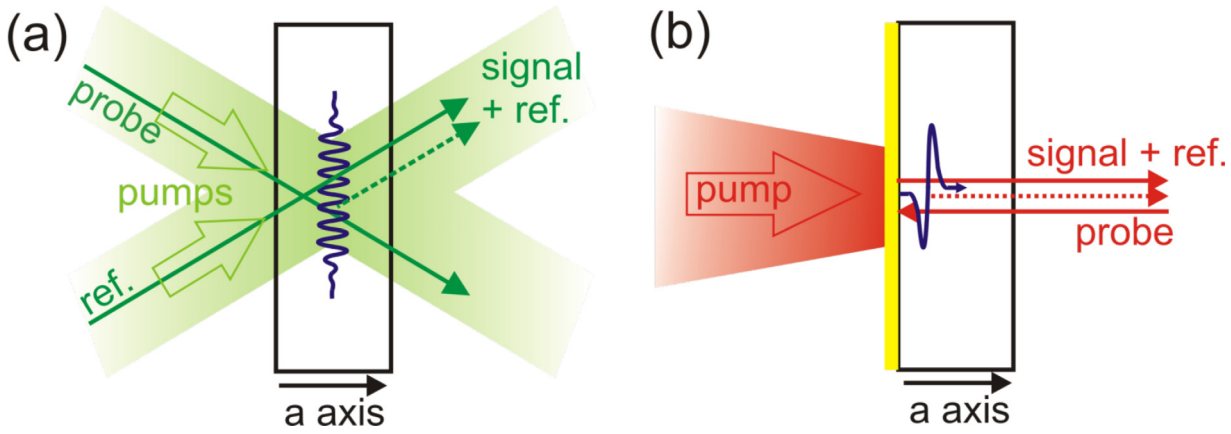

FIG. 1. (Color online) (a) In ISS, optical pump beams with picosecond pulses are crossed to create a spatially periodic, temporally impulsive driving force that launches acoustic waves in the RDX bc-plane. CW probe light diffracted from the acoustic waves is combined with a reference beam and directed to a detector. (b) In PAI, a short pump pulse is focused onto a thin gold transducer. Heating and thermal expansion launch a broadband acoustic strain pulse into the RDX along the axis. A variably delayed femtosecond probe pulse is partially reflected off the acoustic strain pulse and directed to a detector along with light reflected from the gold film that serves as a reference beam.

induced acoustic dispersion by determining the elastic constants at an intermediate frequency of ~450 MHz using impulsive stimulated light scattering (ISS).[16] The ISS-determined elastic constant values were essentially identical to the ultrasound results and significantly different from the BLS results. However, the acoustic frequency of the ISS measurements was too low to conclusively rule out the possibility of relaxation coupling to GHz frequency acoustic waves in RDX. The confirmation of such dispersion in energetic materials could lead to deeper understanding of energy transfer pathways involved in the initiation of detonation, thus emphasizing the need for a number of experimental methods that together continuously cover a broad range of frequencies from the kilo- to terrahertz ranges, essentially across the entire Brillouin zone. In this work, we take steps in this direction by utilizing ISS and picosecond acoustic interferometry (PAI)[17] to measure the quasi-longitudinal speed of sound in single crystal RDX at acoustic frequencies spanning the frequency gap between previous ISS (Ref. 15) and BLS (Ref. 9) measurements.

In BLS, ISS, and PAI, the detection mechanism results from light scattering off of acoustic modes. In contrast to BLS that probes incoherent thermally populated acoustic phonons, both ISS and PAI rely on the generation of coherent acoustic waves. In ISS, coherent acoustic phonons of a well-defined wavevector with typical frequency range from megahertz to low gigahertz are generated by crossing laser beams inside a sample. In PAI, a laser beam is focused onto a thin metal film coated on the sample surface that acts as an acoustic transducer, launching an acoustic wave-packet with frequency components potentially up to hundreds of gigahertz into the sample. The specific details of each of our current measurements are described in the following text.

II. EXPERIMENTAL METHODS

A. Sample preparation

RDX crystals have an orthorhombic structure[18] (*Pbca* space group, nine independent elastic constants), with lattice parameters $a = 1.3182$ nm, $b = 1.1574$ nm, and $c = 1.0709$ nm, and a density of 1.806 g/cm^3. Single crystal samples were prepared at the Los Alamos National Laboratory Energetic Materials Crystal Laboratory as previously described in detail.[19] Briefly, the RDX crystals were grown by evaporation using an acetone solution reflux technique. The crystals were oriented to 1.85° from (100) normal using x-ray diffraction and were cut into thin (~1 mm) slabs with a diamond wire saw. The slabs were polished to an optical finish using an aluminum oxide slurry (1 μm final grit size) in aqueous detergent. For PAI measurements, a thin (~100 nm) gold film was deposited by thermal evaporation on the surface of the RDX crystal.

B. ISS technique

Impulsive stimulated light scattering has been described in more detail previously.[15,16] In the present ISS experiments, a short-pulsed excitation laser beam ($\lambda_e = 515$ nm, 60 ps pulse width, 1 kHz repetition-rate), derived through second harmonic generation of an amplified Yb:KGW laser system (HighQ femtoRegen), was split with a diffractive optic (a binary phase mask pattern) into two beams, which passed through a two-lens telescope and were focused to a 300 μm 1/e beam radius and crossed with external angle θ_e in the sample as depicted in Fig. 1(a). Interference between the two beams created a spatially periodic intensity and absorption pattern with the interference fringe spacing

$$\Lambda = 2\pi/q = \lambda_e/(2\sin(\theta_e/2)). \quad (1)$$

Laser-induced electrostriction (i.e., impulsive stimulated Brillouin scattering[20]) as well as periodic absorption, heating, and rapid thermal expansion (impulsive stimulated thermal scattering[21]) generated coherent, counter-propagating acoustic waves with the wavelength Λ and wavevector magnitude q. The thermal expansion-induced driving force depends on the absorption at the pump wavelength, while the electrostrictive driving force depends on the relevant photoelastic constants and scales with

wavevector.[22] For the highest wavevectors in our current measurements, the electrostrictive force dominates, whereas at lower wavevectors, it accounts for less than half of acoustic wave generation. Strain-induced changes in the refractive index due to the acoustic waves gave rise to time-dependent diffraction (i.e., coherent scattering) of an incident continuous wave probe beam ($\lambda_p = 532$ nm, Coherent Verdi V5 single-longitudinal-mode, intracavity frequency-doubled Nd:YAG laser output, 150 μm beam radius). The probe beam was split into two parts (probe and reference), which were recombined at the sample (focused to 150 μm beam radius) using the same diffractive optic and two-lens telescope used for the excitation beams, ensuring that the probe beam was incident on the spatially periodic acoustic wave "grating" at the Bragg angle for diffraction and that the diffracted signal was superposed with the reference beam for heterodyne detection.[23] Thus Eq. (1) holds for excitation parameters as well as the probe and reference wavelength λ_p and angle of intersection θ_p (i.e., scattering angle). The signal and references beams were directed to a fast detector (New Focus 1591, 4.5 GHz bandwidth) and the time-dependent acoustic oscillations were recorded on an oscilloscope (Tektronix TDS 7404, 4 GHz bandwidth).

C. PAI technique

The sound velocity at ~15 GHz was obtained using picosecond acoustic interferometry (PAI)[17] as depicted in Fig. 1(b). A ~100-nm gold film was deposited onto one face of a (100) RDX crystal. Laser light from an amplified Ti:Sapphire system (Coherent RegA, $\lambda = 790$ nm, 300 fs pulse duration, 250 kHz repetition rate) was split into excitation and variably delayed probe beams. The excitation beam was attenuated to 6 mW to reduce sample heating and focused to a 45 μm beam radius on the free surface of the gold film, which due to rapid heating and thermal expansion acted as a transducer launching an acoustic wavepacket with broadband frequency components that propagates into the RDX along the *a* axis. The probe beam, attenuated to 3 mW, entered the crystal at normal incidence and was focused on the back surface of the gold film to a 25 μm beam radius. The probe reflection from the gold film (reference beam) interferes with coherent backscattering signal light from the acoustic wave as it propagated through the sample, creating a time dependent oscillation in the intensity of the reflected beam at the detected acoustic frequency. The signal and reference light was directed to a photodectector and the signal was collected with a lock-on amplifier at the frequency of an acousto-optic chopper in the excitation beam. The probe wavelength and scattering angle selected a well defined acoustic wavelength given by

$$\Lambda = 2\pi/q = \lambda_p/(2n\sin(\theta_p/2)), \tag{2}$$

where λ_p is the probe wavelength, θ_p is the internal scattering angle, and n is the refractive index. We note that Eq. (2), which determines the acoustic wavelength probed in PAI, is similar to Eq. (1), which determines the acoustic wavelength in ISS. The only difference is that in PAI the probe beam enters and leaves the crystal from the same face so the refractive index must be accounted for in relating the acoustic wavelength in the crystal to the optical wavelength in air. In ISS, this is not necessary because refraction of the incident beams as they enter the crystal compensates for the shorter light wavelengths in the crystal, yielding the same interference fringe-spacing in the crystal as would be produced in the air. The acoustic wavelength probed in PAI through coherent backscattering could be generated through ISS measurements with counter-propagating excitation beams entering the crystal from opposite faces, but it is more convenient to conduct ISS measurements with all the beams entering the same crystal face (yielding a minimum acoustic wavelength of about 1 μm in practice). We thus conduct PAI measurements to probe the smallest PAI acoustic wavelength (highest frequency) of $\Lambda = \lambda_p/2n$. PAI measurements can be conducted with smaller probe scattering angles to select longer wavelengths and lower frequency components of the photo-induced broadband acoustic wavepacket, but experimental difficulties arise at small internal angles. Due to these details, PAI and ISS are complementary techniques for accessing acoustic wavelength ranges of 250–350 nm and 1–100 μm, respectively, with our current pump and probe wavelengths.

III. RESULTS AND DISCUSSION

Figure 2(a) shows ISS data recorded with an acoustic wavelength of 1.8 μm. At $t = 0$, the pump pulses cross in the sample, generating a spike due to instantaneous non-resonant electronic responses in the sample, followed by damped acoustic oscillations. The inset shows the Fourier transform of the data giving a very sharp peak just below 2 GHz. For quantitative analysis, the data are fit in the time domain to a damped sinusoid to recover the acoustic frequency ν, and the quasi-longitudinal speed of sound $V = \nu\Lambda$ is determined using the experimentally set acoustic wavelength Λ given in Eq. (1). In practice, the acoustic wavelength was ascertained from the binary phase mask period and the two-lens telescope imaging. The previous ISS measurements were all conducted with an imposed wavelength of 7.2 μm corresponding roughly (depending on the speed of sound along a particular direction in the anisotropic crystal) to a longitudinal frequency of 450 MHz. To achieve higher acoustic frequencies, we collected data with 10 acoustic wavelengths ranging from 6.6 μm down to 1.0 μm corresponding to acoustic frequencies from 490 MHz to 3.4 GHz. Data were collected in the (100) crystal at a number of different angles corresponding to acoustic waves traveling along different directions in the bc plane.

Figure 2(b) shows the time-derivative of the PAI signal. Laser heating-induced changes in reflectivity of the transducer lead to a large thermal background that can be minimized by taking the derivative of the signal. The inset shows a strong peak at 14.9 GHz in the Fourier transform. The speed of sound V was determined by $V = \nu\Lambda$ using the acoustic wavelength given in Eq. (2) with $\theta_p = 180°$ and $n(790\text{ nm}) = 1.56$. Linear extrapolation of refractive index data in the visible region (450–670 nm) (Ref. 24) was used to estimate n at the probe wavelength. The lack of absorption

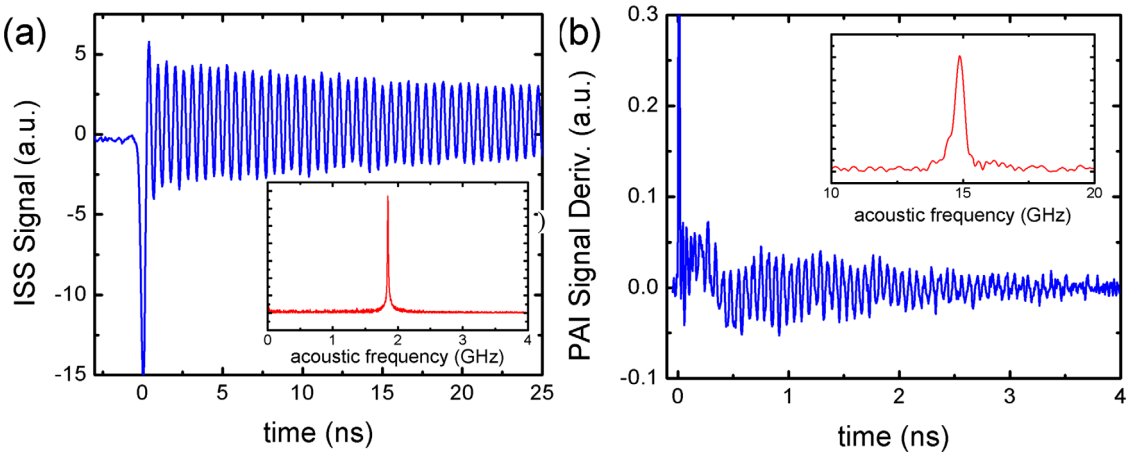

FIG. 2. (Color online) (a) Example of ISS signal. At $t = 0$, pump beams cross in the sample, here generating 1.8 μm wavelength acoustic waves. The inset shows the Fourier transform of the data displaying a sharp peak 1.85 GHz. (b) Time derivative of PAI signal. The signal derivative minimizes the large thermoreflectance background so acoustic oscillations are apparent. The inset shows a peak in the Fourier domain at 14.9 GHz.

bands in the visible[25] and the small index variation observed in this wavelength range validates this procedure.

In Fig. 3, we present digitized data from Refs. 9 and 15 alongside our new ISS and PAI results. We see that for all acoustic wavelengths and frequencies, there is good agreement with previously measured speeds of sound from ISS[15] and ultrasonic[12] techniques. For example, using ISS we measure an acoustic frequency of 2.91 GHz at acoustic wavelength 1.15 μm along the *b* axis (0° in Fig. 3(a)), corresponding to a speed of sound of 3350 m/s, which is very close to 3340 m/s from Refs. 12 and 15. PAI along the *a* axis (0° in Fig. 3(b)) determines the speed of sound to be 3790 m/s at 14.9 GHz, also in good agreement to 3750 m/s from Ref. 15 and 3700 m/s from Ref. 12. Our data do not suffice for the determination of the full set of elastic constants of RDX at any given frequency; however, close agreement with previous ISS and ultrasonic data at all frequencies and directions measured suggests that other crystal orientations and directions should also yield similar results and elastic constant values. In contrast, we see significant disagreement between our ISS and PAI data and the reported BLS results. For example, Ref. 9 reports much higher values of the speed of sound: 3750 m/s for the *b* axis and 4500 m/s for the *a* axis.

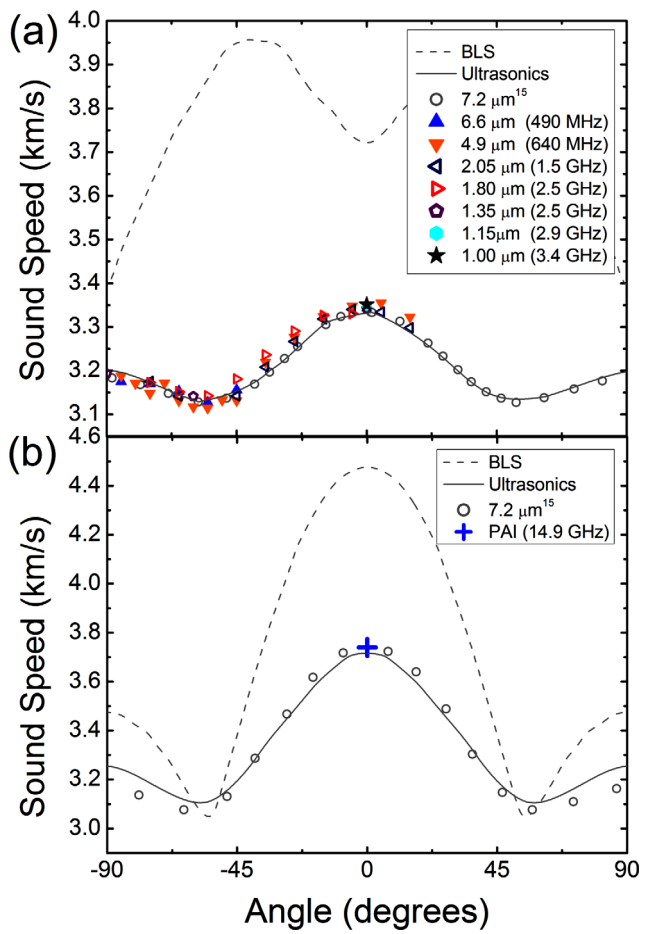

FIG. 3. (Color online) ISS (a) and PAI (b) measured quasi-longitudinal speed of sound along different crystal axes of RDX together with previously published ISS (Ref. 15) (open circles), ultrasonics (solid line), and BLS data[9] (dashed line). Degrees are counted from the *b* axis in (a) and from the *a* axis in (b).

Altogether, we observe good agreement between previously measured anisotropic speeds of sound[11,12,15] from acoustic frequencies of 100 kHz up to 450 MHz and our new ISS and PAI results from 490 MHz up to 14.9 GHz. The lack of acoustic dispersion is strong evidence against any kind of relaxation process coupling significantly to acoustic waves in this frequency range. We are not certain of the reason for the disagreement between these results and the reported BLS results.[9]

IV. CONCLUSIONS

Discrepancies in the reported speeds of sound in RDX from BLS and other techniques have prompted the discussion of possible relaxation processes coupling to acoustic waves at high frequencies. We report new measurements made using ISS and PAI spanning acoustic frequencies from 490 MHz up to 14.9 GHz. These results are in agreement with previous ultrasonics and ISS measurements[11,12,15] at lower frequencies. The lack of acoustic dispersion is persuasive evidence that there is no relaxation process that couples

significantly to linear acoustic waves in RDX at acoustic frequencies from 100 kHz up to 15 GHz.

Although we have extended measurements of the speed of sound in RDX to cover acoustic frequencies over six orders of magnitude, these results do not rule out the possibility of an internal molecular relaxation process coupling to acoustic waves at higher frequencies. Nor do they shed light on potential coupling of large amplitude non-linear acoustic and shock waves to molecular modes that would be involved in detonation. Extending acoustic measurements of energetic materials to higher frequencies (up to THz) as well into the non-linear acoustic and shock domains presents exciting challenges for future research.

ACKNOWLEDGMENTS

This material is based upon work supported under ONR Grant No. N00014-06-1-0459. Crystal growth capabilities were supported at Los Alamos National Laboratory by National Nuclear Security Administration Science Campaign 2.

[1]J. B. Bdzil and D. S. Stewart, Annu. Rev. Fluid Mech. **39**, 263 (2007).
[2]S. M. Walley, J. E. Field, and M. W. Greenaway, Mat. Sci. Tech. **22**, 402 (2006).
[3]S. Zeman, Struct. Bond. **125**, 195 (2007).
[4]R. G. Leisure and F. A. Willis, J. Phys. Condens. Matter **9**, 6001 (1997).
[5]J. M. Brown, E. H. Abramson, and R. J. Angel, Phys. Chem. Miner. **33**, 256 (2006).
[6]R. Vacher and L. Boyer, Phys. Rev. B **6**, 639 (1972).
[7]A. G. Every, Meas. Sci. Technol. **13**, R21 (2002).
[8]A. A. Maznev, A. Akthakul, and K. A. Nelson, J. Appl. Phys. **86**, 2818 (1999).
[9]J. J. Haycraft, L. L. Stevens, and C. J. Eckhardt, J. Chem. Phys. **124**, 024712 (2006).
[10]L. L. Stevens, D. E. Hooks, and A. Migliori, J. Appl. Phys. **108**, 053512 (2010).
[11]S. Haussühl, Z. Kristallogr. **216**, 339 (2001).
[12]R. B. Schwarz, D. E. Hooks, J. J. Dick, J. I. Archuleta, and A. R. Martinez, J. Appl. Phys. **98**, 056106 (2005).
[13]K. F. Herzfeld and T. A. Litovitz, *Absorption and Dispersion of Ultrasonic Waves* (Academic Press, New York, 1959).
[14]J. E. F. Rubio, M. Taravillo, V. G. Baonza, J. Núñez, and M Cáceres, J. Chem. Phys. **124**, 014503 (2006).
[15]B. Sun, J. M. Winey, N. Hemmi, Z. A. Dreger, K. A. Zimmerman, Y. M. Gupta, D. H. Torchinsky, and K. A. Nelson, J. Appl. Phys. **104**, 073517 (2008).
[16]K. A. Nelson, D. R. Lutz, L. Madison, and M. D. Fayer, Phys. Rev. B **24**, 3261 (1981).
[17]H. N. Lin, R. J. Stoner, H. J. Maris, and J. Tauc, J. Appl. Phys. **69**, 3816 (1991).
[18]C. S. Choi and E. Prince, Acta Cryst. **B28**, 2857 (1972).
[19]D. E. Hooks, K. J. Ramos, and A. R. Martinez, J. Appl. Phys. **100**, 024908 (2006).
[20]Y. Yan, E. B. Gamble, and K. A. Nelson, J. Chem. Phys. **83**, 5391 (1985).
[21]J. A. Rogers, Y. Yang, and K. A. Nelson, Appl. Phys. A **58**, 523 (1994).
[22]K. A. Nelson, R. J. D. Miller, D. R. Lutz, and M. D. Fayer, J. Appl. Phys. **53**, 1144 (1982).
[23]A. A. Maznev, J. A. Rogers, and K. A. Nelson, Opt. Lett. **23**, 1319 (1998).
[24]W. C. McCrone, Anal. Chem. **2**, 81 (1941).
[25]V. H. Whitley. AIP Conf. Proc. **845**, 1357 (2006).